UNIVERSITY OF AMSTERDAM

UvA-DARE (Digital Academic Repository)

Angle-resolved cathodoluminescence nanoscopy

Coenen, T.

Publication date
2014

Link to publication

Citation for published version (APA):
Coenen, T. (2014). *Angle-resolved cathodoluminescence nanoscopy*. [Thesis, externally prepared, Universiteit van Amsterdam].

General rights
It is not permitted to download or to forward/distribute the text or part of it without the consent of the author(s) and/or copyright holder(s), other than for strictly personal, individual use, unless the work is under an open content license (like Creative Commons).

Disclaimer/Complaints regulations
If you believe that digital publication of certain material infringes any of your rights or (privacy) interests, please let the Library know, stating your reasons. In case of a legitimate complaint, the Library will make the material inaccessible and/or remove it from the website. Please Ask the Library: https://uba.uva.nl/en/contact, or a letter to: Library of the University of Amsterdam, Secretariat, P.O. Box 19185, 1000 GD Amsterdam, The Netherlands. You will be contacted as soon as possible.

UvA-DARE is a service provided by the library of the University of Amsterdam (https://dare.uva.nl)

Download date:04 Nov 2026

7

A planar parabolic antenna

One of the simplest and most common structures used for directing light in macroscale applications is the parabolic reflector. Parabolic reflectors are ubiquitous in many technologies, from satellite dishes to hand-held flashlights. Today, there is a growing interest in the use of ultracompact metallic structures for manipulating light on the wavelength scale. Significant progress has been made in scaling radiowave antennas to the nanoscale for operation in the visible range, but similar scaling of parabolic reflectors employing ray-optics concepts has not yet been accomplished because of the difficulty in fabricating nanoscale three dimensional surfaces. In this Chapter, we demonstrate that plasmon physics can be employed to realize a resonant elliptical cavity functioning as an essentially planar nanometallic structure that serves as a broadband unidirectional parabolic antenna at optical frequencies.

7.1 Introduction

Controlling the far-field emission pattern of nanoscale objects is one of the central goals of optical antennas [29, 168]. In most cases, the desired pattern is a beam of light in the far field, which can couple a nanoscale source or sink of light to a distant object. Optical beaming could improve performance in a variety of important applications, such as photon sources [169], photodetectors [170], sensors [171], and photovoltaics [172]. Previous antennas have demonstrated beaming

in engineered directions over narrow frequency ranges [39, 123, 144, 173–175], or broadband beaming in structures several times larger than the wavelength [176]; however a broadband device with a small footprint and high directivity has not yet been demonstrated. Parabolic reflectors are ubiquitous macroscopic structures that efficiently couple electromagnetic energy from a focal point to a beam and work over a very large range of frequencies. It would seem natural that parabolic structures would also be useful for small-scale optical antennas; however, fabricating complex three-dimensional surfaces is not generally possible with traditional nanofabrication tools. By using a gold surface as a two- dimensional medium for propagation of surface waves, namely, surface plasmon polaritons (SPPs), it is possible to reduce the dimensionality of a parabolic reflector while maintaining its optical beaming behavior. We demonstrate that a two-dimensional cross section of a paraboloid cut into a gold surface, an elliptical cavity, presents the broadband unidirectional emission expected of the full three-dimensional structure and is much more amenable to fabrication. When reduced in size to the wavelength-scale, these structures retain their beaming functionality and also present a set of well-defined optical resonances that enhance emission for particular wavelengths.

Parabolic reflectors are well-known in geometrical optics; they couple the emission of a point source at the parabola's focus to a plane wave propagating parallel to parabola's axis, and *vice versa*. In a classical three-dimensional parabola the emitted light beam originates from the specular reflection of light over the entire parabola's surface. However, due to the special geometrical properties of a parabola, an array of individual scatterers placed in a parabolic arrangement will also generate a parallel beam of light in the far field. In fact, a point source coupled to any two-dimensional subsection of a paraboloidal surface will generate a wave preferentially propagating parallel to the paraboloid's axis. One special case of such a subsection is the elliptical intersection of a paraboloid with a planar surface, with the paraboloid and the planar ellipse sharing a common focus. In such a geometry, a beam of light can be generated by exciting SPPs near one of the two foci inside the planar ellipse followed by coherent scattering of the SPPs to free-space photons via the edges of the area in the form of a collimated beam. The direction of the beam is only determined by the position of the source inside the ellipse and the ellipse's eccentricity. A detailed analytic description of this model is given in the Supporting Information of Ref. [177].

Figures 7.1(a,b) show the sample geometry. A series of concentric elliptical grooves has recently been used to realize a bull's eye type beam director with a controllable beam direction based on a similar concept [178]. In contrast to this work, the elliptical bull's eye structure has a well-defined operation wavelength based on coherent scattering from multiple grooves, whereas here the broad optical resonances of the plasmonic cavity are utilized to achieve high directivities.

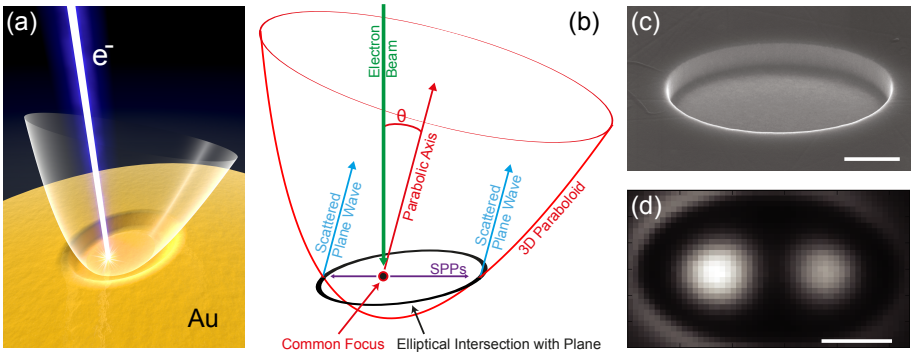


Figure 7.1: (a) 3D Graphical representation of ellips acting as a parabolic antenna (image by Tremani) (b) Schematic of the intersection of a paraboloid with a planar surface, creating an ellipse. (c) SEM image of elliptical arena taken at 52° off the surface normal. The scale bar is 500 nm. (d) 30 keV cathodoluminescence image at a collection wavelength of 720 nm for a 1.0-µm-long, 800-nm-wide elliptical cavity. The scale bar is 250 nm.

7.2 Sample fabrication

The elliptical arenas were fabricated by focused-ion-beam (FIB) milling using an FEI Helios Nanolab Dual Beam instrument into a single crystal pellet of gold which had been previously polished to nanometer-scale roughness. Similar geometries can also be made using template stripping [179]. Patterns were defined as bitmaps and milled top to bottom with a beam current of 1.5 pA. Higher beam currents also provide structures with similar behavior.

7.3 CL imaging of elliptical cavity plasmon modes

A SEM image of a characteristic ellipse is shown in Fig. 7.1(c). Several different elliptical geometries were fabricated with major axis lengths ranging between 500 and 1600 nm, and eccentricities, defined as the ratio between the major axis length and the focus-to-focus distance, between 0 and 1. The depth of the elliptical cavity was also varied; typically a depth of 400 nm was used. The localized optical modes in these structures were determined using our angle-resolved cathodoluminescence imaging spectroscopy (ARCIS) technique (for details on the experimental setup see Chapters 2 and 3). A 30 keV electron beam is raster-scanned over the surface and serves as a broad-band point source of surface plasmon polaritons. The radiation spectrum emitted by the antenna is collected by a half-paraboloidal mirror placed between the microscope's pole piece and the sample, after which the spectrum can be measured with a spectrometer and the angular distribution can be measured with a 2D CCD camera.

Fig. 7.1(d) shows a CL image of a 1000 × 600 nm elliptical cavity recorded at a wavelength of 720 nm. The pixel size in the images of the smaller cavities is 10 × 10 nm and 20 × 20 nm in the largest cavities. The two foci of the elliptical antenna are clearly resolved in the image, demonstrating the subwavelength resolution of the CL technique. As CL is a direct probe of the radiative component of the local density of optical states (LDOS) [63], images such as in Fig. 7.1(d) provide a direct absolute measure of the radiation power of the antenna at any wavelength.

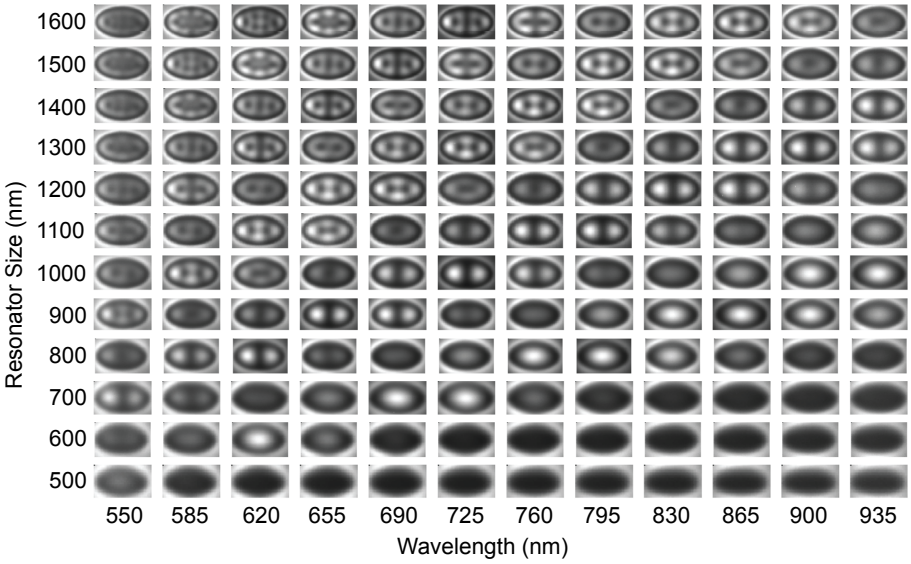


Figure 7.2: Cathodoluminescence images (30 keV electrons) for cavities with eccentricity 0.8 and major axes ranging from 500 to 1600 nm for different collection wavelengths. Cavity modal patterns with increasing mode order ($m = 0, 1, 2, ...$) are clearly visible. All images are scaled by the major axis length.

Figure 7.2 shows CL images for cavities with an eccentricity of 0.8, with major axes between 500 nm and 1.6 μm. Data are shown for collection wavelengths in the range 550 – 935 nm. As can be seen, as the ratio of cavity size to wavelength increases, cavity modal intensity distributions of increasing mode order are observed. Modal distributions of a similar type have previously been observed in plasmonic whispering gallery cavities and cylindrical cavities [165, 180], and the modal distributions of photonic elliptical cavities has been explored by near-field scanning optical microscopy [181, 182]. Fig. 7.3 shows the CL spectra averaged over the elliptical cavity area for the 2D scans presented in Fig. 7.2. It can be seen that the resonant modes shift to longer wavelengths as the cavities increase in size. Different resonant modes, observed in Fig. 7.2, appear as different resonant peaks in the spectra. The quality factor for the plasmon resonances in Fig. 7.2 is in the range $Q = 10 – 20$. Larger cavities have lower quality factors due to increased ohmic

losses of the SPPs in the metal. Resonant modes at long wavelengths have lower Q due to a lower reflection coefficient at the cavity end, caused by a larger modal evanescent tail in the normal direction into the air. Similarly, deeper cavities show higher quality factors due to increased reflectivity of the metallic walls, which lowers the radiation losses (see Supplementary Fig. 7.5).

7.4 Resonance model for ellipses

While an exact analysis of the elliptical cavities resonant modes can be made using a Green's function approach or the boundary-element method [181–183], a first-order model that provides very good physical insight predicts resonances occurring when the phase accumulated by SPPs traveling a round trip inside the ellipse is equal to an integer number m times 2π:

$$2Lk_{SPP} + 2\Phi = 2\pi m \tag{7.1}$$

with L the major axis length, k_{SPP} the SPP wave vector, and Φ the phase increment upon reflection at the cavity boundary. This model describes the cavity modes in one-dimensional nanowires where the resonance are determined by the cavity length [32, 145, 151, 184]. All of the experimentally observed peaks can be fit with this model, even though it only considers resonances related to one characteristic length, that of the major axis. This directly follows from the special geometrical properties of ellipses: in an elliptical cavity, in a simple ray optics picture, all rays that emanate from one focus will reflect off the ellipse's edge in the direction of the opposite focus. The distance of this path is the same regardless of the initial direction of the first ray and is equal to the major axis length. Thus the major axis length defines the characteristic resonances for the cavity. The reflections of SPPs in elliptical cavities have been explored previously by leakage radiation microscopy for large cavities with major axis lengths greater than 30 μm [185], but this is the first time such a model has been proposed for a resonant SPP cavity on the wavelength scale. We approximate the SPP wave vector by that for an SPP propagating on an infinite plane of gold. The wave vector in the ellipse will be affected by the lateral confinement imposed by the walls of the cavity, which explains the shift observed between the predicted peak positions and those in the experiment. The increased confinement experienced by the SPPs in the elliptical cavity will result in increased wave vector, resulting in shorter SPP wavelengths compared to free space than calculated, thus shifting the observed modes to the left in Fig. 7.3(b), closer to the model prediction. Interestingly we do not see spectral evidence of any whispering gallery type modes. It is possible that such modes, if they exist, are confined to the corners of the structure. If so, they will have a mode index substantially higher than those for the SPPs propagating on the floor of the cavity, and thus may radiate poorly to the far field.

Figure 7.3(b) shows the data from Fig 7.3(a) replotted versus plasmon wavelength and cavity length. The linear resonance redshift with cavity length is clearly

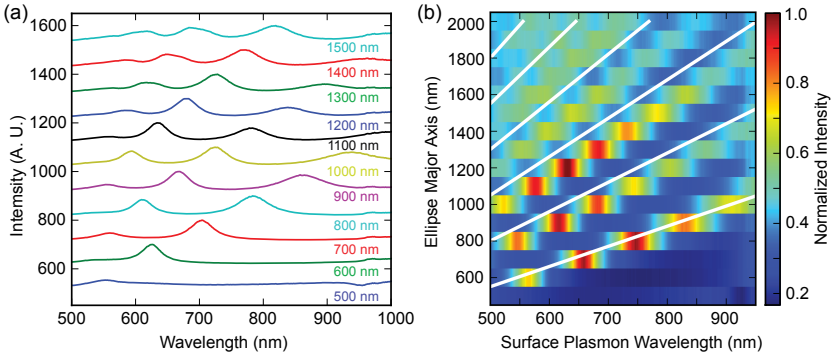


Figure 7.3: (a) Cathodoluminescence spectra for elliptical cavities with eccentricity 0.8 with major axes ranging from 500 to 1600 nm. A redshift for the various resonances increasing cavity size is clearly visible. (b) Same data as in (a) now represented in a map of CL intensity *versus* surface plasmon wavelength and cavity major axis. The white lines indicate the resonant modes calculated using a Fabry-Pérot interference model.

visible (see also Supplementary Fig. 7.6(a)). We fitted Eq. 7.1 through the entire data set for all modes in Fig. 7.3(b), with the phase pickup Φ as the only free parameter, which yields the white dashed lines in Fig. 7.3(b). The model describes the overall trends very well (also see Supplementary Fig. 7.6(b)) and yields $\Phi = -1.2\pi$. The negative value obtained for Φ is in contrast to experiments on strip antennas which have shown a positive phase pickup [150, 151]. The negative phase pickup for an SPP reflecting off the metallic ellipse boundary is similar in nature to the negative phase pickup seen for a plane wave reflection off a metal mirror. This phase shift effectively makes the arena appear smaller than would be expected for a phase pickup $\Phi = 0$. This attenuation in the spatial extent of the modes is also clearly visible in the modal distributions in Fig. 7.2, in which a band of low CL signal is observed on the inside edges of the cavities for all modes and cavity sizes.

Figure 7.4 shows the angular distribution of light emitted by the cavities in terms of the directivity at these angles. The directivity of an antenna is related to an antenna's ability to radiate light in a particular direction:

$$D(\theta,\phi) = \frac{4\pi}{P_{rad}} p(\theta,\phi) \tag{7.2}$$

where the directivity D is given as a function of azimuthal and zenithal angle and is proportional to the emitted power p at these angles normalized by the total radiated power P_{rad} per solid angle. Data are shown for elliptical cavities with eccentricity of 0.8 and major axes of 1.1, 1.3, and 1.5 µm. Figures 7.4(a-c) show the CL intensity maps for the resonances nearest 600 nm for each cavity: at 628 nm, 609 nm, and 589 nm, respectively. Figures 7.4(d-f) show the angular emission patterns collected for e-beam excitation of the antenna in the outermost antinode in the

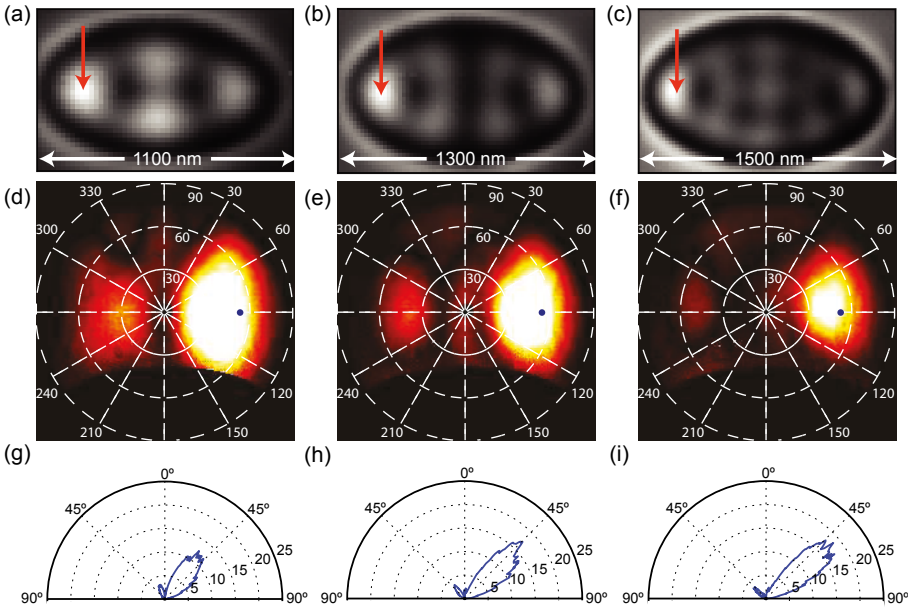


Figure 7.4: (a-c) Cathodoluminescence images of elliptical antennas with eccentricity 0.8 and major axes of 1100, 1300, and 1500 nm taken at resonance wavelengths of 628 nm, 609 nm, and 589 nm, respectively. The images are scaled by the major axis length. (d-f) Normalized angular emission collected using a 40 nm band-pass filter centered at 600 nm for the three cavities taken using electron beam excitation at the modal maxima in (a) (see arrows). Blue dots indicate the paraboloid axis for each structure. (g-i). Line cuts at the azumithal angle of peak emission with the data normalized as directivity. The maximum directivity in panel (i) is 18.

resonant modal intensity pattern. Clear beaming of light of these resonant modes at an azimuthal angle $\phi = 90^\circ$ and zenithal angle $\theta = 52^\circ$ is observed. Our model predicts the angle to be 53.1° for this eccentricity, in reasonable agreement. The smallest half-width-at-half-maximum (HWHM) is found in the largest cavity: 17° and 24° for the azimuthal and zenithal angles, respectively. Figures 7.4(g-i) show cuts of the angular emission distribution in the zenithal angular emission lobe, with the radial scale plotted as emission directivity, that is, the emission normalized by an isotropic emitter of the same total power. We find that the maximum observed directivity is 18 for the 1.5 μm antenna. This value compares favorably to other wavelength scale devices, such as the nanoscale Yagi-Uda antenna [39], but is clearly lower than structures that are larger in size such as the bull's eye directors [174]. This trade-off is evident in our own observation that larger structures give higher directivities. In the end there will always be a trade-off between absolute size and the maximum achievable directivity related to the diffraction of

the emitted light.

The data in Fig. 7.4 clearly show the strong directivity of the elliptical antenna, a unique feature given its planar geometry. It is the result of the constructive interference in the far-field of surface plasmon polaritons that are coherently scattered off the boundary of the elliptical cavity. The operation wavelength and outcoupling angle can be tuned by varying the ellipses' geometrical size and eccentricity (see Supplementary Fig. 7.7). The main emission near $\theta = 53^\circ$ observed in Fig. 7.4 corresponds well to the optical axis of a paraboloid intersecting with the gold surface, with the focal point at the position of the electron beam impact, as indicated in Fig. 7.4(a). E-beam illumination of the area around the foci which appear bright in the LDOS map (Figs. 7.4(a-c)) leads to a "forward" directed beam in the far field. This work thus provides a demonstration of the coupling of the two-dimensional optical "flatland" with the three-dimensional far field. A central advantage of this type of antenna is that every resonant mode directs energy in the same direction, as can be observed for the three modes in Fig. 7.4. In contrast, many other antenna designs will only broadcast in the "forward" direction for a single designed frequency. In this sense, the antenna is "broadband". Of course, strong LDOS enhancement is only available when the structure is on resonance, so the most accurate description is that the antenna has several operating bands, each of which broadcasts energy in the forward direction. Since this is a plasmonic cavity with a moderate Q, these bands are not narrow but have a bandwidth of about 50 nm and are tunable by varying the size of the ellipse. Another distinct feature of these elliptical antennas is that the volume from which emitters can couple is relatively large, that is, on the order of a wavelength cubed. This can be contrasted with the Yagi-Uda antenna composed of an array of coupled metal nanoparticles [39, 123]. Such an antenna (which shows a similar angular spread as the elliptical antennas presented here) has an approximately 2 orders-of-magnitude smaller volume from which emitters can efficiently couple to the antenna's radiation field as that is determined by the optical near-field of one metal nanoparticle, typically a shell with a thickness of only ~20 nm around the "feed" particle (see Section 7.6.2 in the Supplementary information). In many applications where precise positioning of the local emitter is impossible or difficult, this will be a significant advantage. Furthermore, taking advantage of the fact that SPPs can be excited electrically [41], and the fact that electrical circuitry can be integrated with the planar antenna geometry, this design may pave the way for electrically driven directional optical antenna emitters. Finally we note the application of these elliptical antennas in the receiving mode, for example, in photodetectors and solar cells, in which light with different colors can be selectively collected and converted to electrical current at distinct regions inside the cavity.

7.5 Conclusions

In conclusion, we have demonstrated a novel antenna design, a resonant elliptical cavity, that enables the controlled coupling of optical emitters to the far-field at a well-defined angle. The emission is due to the excitation and coherent scattering of surface plasmon polaritons to the far field at optical resonances with $Q = 10 - 20$. The cavity has strong directivity (18) and has a corresponding optical volume that is more than 100 times larger than that of an optical Yagi-Uda antenna. The direction and wavelength of operation of the antenna can be controlled by simple geometric parameters. This work demonstrates the possibility of integrating "flatland" optics with the far-field, namely, the control of three-dimensional electromagnetic radiation by two-dimensional resonant structures. This could lead to important applications in a large variety of technology areas, including lighting, photodetectors, quantum optical circuitry, and photovoltaics.

7.6 Supplementary information

7.6.1 Supplementary figures

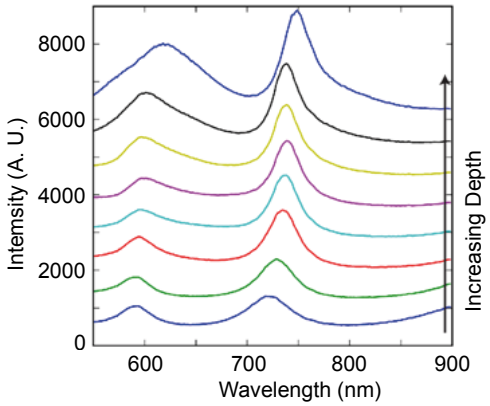


Figure 7.5: Resonator linewidth *versus* depth. Cathodoluminescence spectra collected for arenas with major axis length 1 µm and eccentricity 0.8, for structures with depths ranging from 200 nm to 1 µm. The resonance linewidth increases for increasing depth due to the higher reflectivity of the cavity wall.

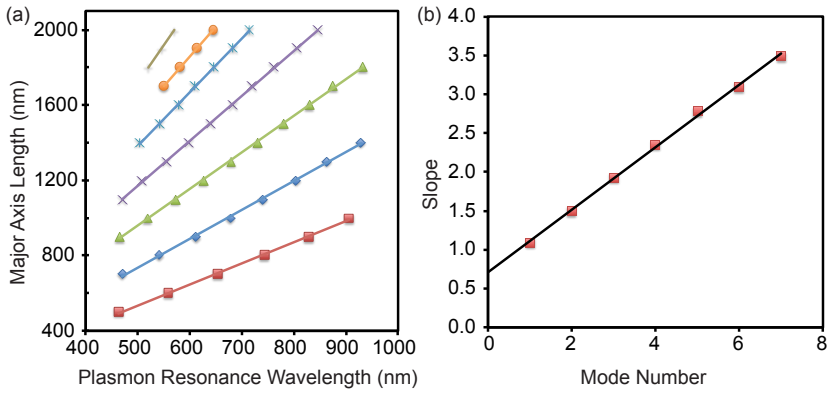


Figure 7.6: Extraction of the phase pickup on reflection. (a) Surface plasmon resonance wavelengths *versus* cavity major axis length for resonators with major axis lengths ranging from 500 nm to 2000 nm, assuming the dispersion relationship for a planar film of gold. A linear relationship between resonator size and the resonant plasmon wavelength is observed, with increasing slope for higher order resonances, in agreement with Eq. 7.1. (b) Slope of the lines in (a) for the subsequent modes. A linear increase of the slope with mode number is observed, in agreement with Eq. 7.1. The intercept with the ordinate of the line fitted through the data is 0.60, corresponding to a phase shift $\Phi = -1.2\pi$.

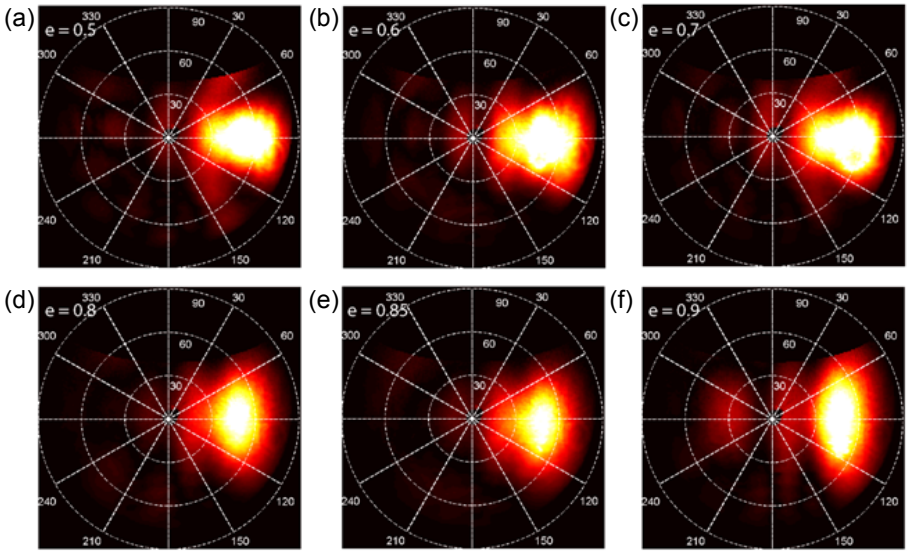


Figure 7.7: Angular radiation patterns as a function of eccentricity. Data are shown for structures with a major axis length of 1 μm and eccentricities (indicated in the panels) in the range 0.5 – 0.9

7.6.2 Calculation of effective coupling volume

In the Chapter it is claimed that the effective coupling volume, *i.e.* the volume in which an emitter will couple well to the antenna modes, is 100 times larger than that quoted recently for a nanoscale Yagi-Uda antenna [39]. In order to calculate this volume, one needs to consider the FWHM of the LDOS antinodes parallel and perpendicular to the long axis, as well as the decay of the SPP mode into the air above the plane of the elliptical cavity. As we assumed for calculating the SPP dispersion in the Fabry-Pérot model, we here assume the dispersion relationship for the SPPs in the structure to be that for a semi-infinite plane of gold. In this case, the decay length of the SPP into the air is given by following the well-known equation:

$$z_{air} = \frac{\lambda_0}{2\pi}\left(\frac{|\varepsilon'_{metal}| + \varepsilon_{air}}{\varepsilon^2_{air}}\right)^{1/2} \tag{7.3}$$

We then make the approximation that the volume is a half ellipsoid with semi-axis lengths given by the x and y HWHM values and the z_{air} given above. For the 1.3 micron ellipse at 600 nm wavelength these values are 106 nm, 86 nm, and 293 nm, for x, y and z, respectively, giving a volume of approximately 5.6×106 nm^3. In contrast, other antennas such as the Yagi-Uda require near-field coupling to a local element, which can only occur when the emitter is placed within a few tens of nanometers from the appropriate position. If we assume this corresponds to a sphere of radius 25 nm, the corresponding coupling volume is 3.27×104 nm^3, or 171 times smaller than that for the elliptical cavity antenna. In reality, good near-field coupling usually requires even more precise localization of the emitter, so the ratio is actually much larger. However, a conservative claim of 100 times is justified.